

Accretion disk reversal and the spin-up/spin-down of accreting pulsars

James R. Murray, Martijn de Kool and Jianke Li

Astrophysical Theory Centre¹, Australian National University, ACT 0200, Australia

ABSTRACT

We numerically investigate the hydrodynamics of accretion disk reversal and relate our findings to the observed spin-rate changes in the accreting X-ray pulsar GX 1+4. In this system, which accretes from a slow wind, the accretion disk contains two dynamically distinct regions. In the inner part viscous forces are dominant and disk evolution occurs on a viscous timescale. In the outer part dynamical mixing of material with opposite angular momentum is more important, and the externally imposed angular momentum reversal timescale governs the flow. In this outer region the disk is split into concentric rings of material with opposite senses of rotation that do not mix completely but instead remain distinct, with a clear gap between them. We thus predict that torque reversals resulting from accretion disk reversals will be accompanied by minima in accretion luminosity.

Subject headings: accretion, accretion disks — binaries: general — hydrodynamics — methods: numerical — pulsars: individual (GX 1+4) — stars: rotation

¹Operated jointly by Mount Stromlo and Siding Spring Observatories & School of Mathematical Sciences, The Australian National University, ACT 0200, Australia

1. Introduction

The availability of continuous monitoring data for several X-ray pulsars as obtained with the BATSE All Sky Monitor on the Compton Gamma Ray Observatory over the last five years (Bildsten et al. 1997, Nelson et al. 1997) has led to renewed interest in the spin evolution of accreting neutron stars with a strong magnetic field. From earlier pointed observations of X-ray pulsars with other satellites it was already known that the spin rates of these neutron stars show changes on many timescales, ranging from unresolved fluctuations (shorter than 1 day) to systematic trends lasting over decades (see, e.g. the compilation by Nagase 1989).

X-ray pulsars are usually divided into two groups, those which accrete from a Roche-lobe filling companion by way of an accretion disk, and those that accrete from the stellar wind of a companion star, in which case a disk may or may not be present. The second group tends to show more erratic spin rate changes on longer timescales, whereas the disk accreting pulsars generally show long term systematic trends. On the shortest timescales however the spin rate changes in the two groups appear to be comparable (de Kool & Anzer 1993, Baykal & Ögelman 1993).

Several models have been proposed to explain these spin rate fluctuations, or alternatively the torques that cause them. In the standard disk accretion model (Ghosh & Lamb 1979) the pulsars are spinning at an equilibrium period, at which the spin-up torque due to the angular momentum of the accreting material (often referred to as the material torque) and the interaction of the magnetic field of the pulsar with the disk inside the co-rotation radius is balanced by a braking (spin-down) torque due to the interaction with the more slowly rotating outer parts of the accretion disk. The equilibrium period depends on the accretion rate, and the pulsar is expected to spin-up or down as the accretion rate increases or de-

creases. This model appears consistent with the observed positions of X-ray pulsars in the pulse period - X-ray luminosity (equivalent to accretion rate) diagram. It also explains why the long term spin rate changes are considerably smaller than what would be expected from the material torque alone.

However, the standard disk accretion model does not explain the spin rate fluctuations observed on very short timescales that are superposed on the long timescale trends in most disk accreting sources. These fluctuations must be caused by torques that are as strong as the full material torque, much larger than the net torques expected to result from a small disequilibrium between spin-up and spin-down torques.

For the wind-accreting pulsars, a different mechanism can be invoked to explain the positive and negative spin rate changes. Early numerical studies of Bondi-Hoyle accretion flow (e.g. the two dimensional simulations by Matsuda et al. 1987, Fryxell & Taam 1988, 1989) demonstrated that it may be possible to form temporary accretion disks with alternating senses of rotation in a wind accreting system. More recent high resolution three dimensional numerical investigations of the so-called wind “flip-flop” instability may be found in Ruffert (1992, 1997) and the references therein. The timescale of the disk reversals is found to be of the order of the sound crossing time of the accretion radius, which for the most common systems in which the neutron star accretes from a fast wind from an early type (O or Be) star is of the order of hours. This is consistent with the torque fluctuations observed in wind accreting sources, which also appear to be of the order of the material torque discussed above, but applied in random directions with the direction changing on a timescale shorter than 1 day.

The new continuous monitoring data obtained by BATSE (Bildsten et al. 1997, Nelson et al. 1997, Chakrabarty et al. 1997) have yielded values for the mass accretion rate (X-ray luminos-

ity) and the accretion torque (change in spin frequency) on a regular basis for a large number of X-ray pulsars. This data set has allowed a detailed comparison of the observed relation between accretion rate and torque, and that predicted by theoretical models. (It should always be kept in mind however that the fluxes measured by BATSE are only the *pulsed* fraction of the X-ray luminosity, and that it is not clear whether the ratio between pulsed and non-pulsed fluxes is constant).

The observations are not consistent with the standard Ghosh & Lamb model, since this predicts a clear correlation between spin-up and an increase in X-ray luminosity, whereas the observations show a variety of behaviour, with spin-up or spin-down occurring at the same apparent luminosity. The cause of this type of behaviour in disk accreting systems is not well understood, but a possible explanation has recently been suggested by some of us (Li & Wickramasinghe 1998).

However, for wind accreting systems the possibility of accretion from temporary accretion disks with alternating senses of rotation is still tenable. In analogy, Nelson et al. (1997) made the *ad hoc* suggestion that many observational features of some systems that are normally thought to contain disks (GX 1+4, 4U 1626-67) would be explained if they were accreting from disks with alternately prograde and retrograde senses of rotation. Previously, Makishima et al. (1988), Dotani et al. (1989) and Greenhill et al. (1989) had also sought to explain the rapid spin-down of GX 1+4 in terms of accretion from a retrograde disk.

If the secondary star is feeding the accretion disk via Roche lobe overflow, as is almost certainly the case in 4U 1626-67, it is hard to conceive how a retrograde disk could ever come about. However, in the case of GX 1+4, the suggestion is not unreasonable. This X-ray pulsar is unique in the sense that it is accreting from a red giant or AGB star wind (Chakrabarty & Roche

1997), and is in a very wide orbit. Estimating the timescale of disk reversal for accretion from such a wind, one obtains a timescale of the order of years, and the disk would form at a large radius ($\sim 10^{13}$ cm) so that the inner part of the accretion flow is expected to be like a normal accretion disk. A timescale of years corresponds well with the timescale on which the accretion behaviour in GX 1+4 is observed to change, with a negative correlation between accretion rate and spin-up in some phases while the disk would be retrograde, and a positive one at other times when it is prograde (Chakrabarty et al. 1997). Thus, this system is ideally suited to study the possibility of forming retrograde disks, since the timescale for disk reversal would be much longer than that of the torque fluctuations on a timescale of one day or less that are common in all types of X-ray pulsars. In the systems that accrete from a fast wind, the two timescales are comparable, and the effects will be difficult to separate.

Relatively little modelling of the hydrodynamics of disk reversal has been performed, making it difficult to assess whether this model is in agreement with the observations. The previous numerical studies of Bondi-Hoyle accretion flow (e.g. Ruffert 1997, Matsuda et al. 1987) did not resolve the inner part of the accretion disk, and did not yield much insight in such details as the interaction of an existing disk with material coming in with opposite angular momentum, the timescales determining the evolution of such systems, and the relation between accretion torque and luminosity expected in such a model.

In this paper we use Smoothed Particle Hydrodynamics (SPH) simulations to start an investigation into these processes, and compare our results with the observation of GX 1+4.

2. Numerical Results

2.1. Numerical Method

The aim of the calculations described here is to investigate the response of an accretion disk

to a change in the specific angular momentum of the material it is being fed. In particular we are interested in the case where the specific angular momentum of the material added at the disk's outer boundary is reversed.

The simulations were performed using an SPH code that has been specifically adapted for disk problems (Murray 1996). Two and three dimensional applications of the code can be found in Murray (1998) and Murray & Armitage (1998). To control the computational expense, motion perpendicular to the disk plane was neglected, and the calculations were run in two dimensions. We took full advantage of the adaptive nature of SPH and allowed the particle smoothing length (and hence the resolution) to vary in space and time.

Viscous dissipation is included in the code using a linear term in the SPH equations that is based upon the linear artificial viscosity term described in Monaghan (1992). Detailed descriptions and tests of the term's application to accretion disks are to be found in Murray (1996, 1998). In the continuum limit this dissipation term introduces a viscous force per unit mass

$$\mathbf{a}_v = \frac{\zeta h}{8\Sigma} (\nabla \cdot (c\Sigma\mathbf{S}) + \nabla(c\Sigma\nabla \cdot \mathbf{v})), \quad (1)$$

where \mathbf{S} is the deformation tensor, Σ is the column density, h is the smoothing length, c is the sound speed, and ζ is the SPH linear artificial viscosity parameter. In this work we have simply set $\zeta = 1$. In the simulations described below, both the density and the sound speed vary on similar spatial scales to the velocity. Hence we cannot (as was previously done in e.g. Murray 1998) approximate the dissipation in equation 1 as the sum of a shear and a bulk viscosity.

2.2. Simulation Details

We simulated the gas flow in the annular region $r_{\text{in}} < r < r_{\text{inj}}$. r_{inj} is the radius at which gas is added to the simulation. Ideally we should like r_{in} to be of the order of the magnetospheric

radius r_m (a radius characterising the truncation of the viscous accretion disc), and r_{inj} to be of the order of 0.1 times the accretion radius,

$$r_{\text{acc}} = GM/v_w^2,$$

where G is the gravitational constant, M is the mass of the neutron star, and v_w is the wind velocity. Indeed for sources accreting from a fast wind the disk formation radius is not much larger than r_m and it is computationally feasible to simulate the entire region $r_m < r < 0.1 r_{\text{acc}}$.

However, for the system GX 1+4, the accretion radius is several orders of magnitude larger than r_m , and we can not resolve the full range in radius over which the disk is likely to extend. We have worked around this problem in the following way. As discussed in the next section, we expect the disk to be divided in two parts, an inner one in which viscous forces dominate, and an outer one in which dynamical mixing of material with opposite angular momentum is more important. We therefore consider two cases, one with a very low viscosity which should apply to the outer regions of the disk, and another with much higher viscosity which models the parts of the disk where the transition from dynamical mixing to viscous transport occurs. Although this still does not cover the range in radius all the way down to the magnetospheric radius, we can expect that inside the transition region a standard accretion disk is present which adjusts instantaneously to its outer boundary condition.

The gravitational potential was simply taken to be that of the accreting star, thereby neglecting tidal effects. This is likely a very good approximation, since the hydrodynamical simulations of the flip-flop instability show that disk formation generally occurs at $r \sim 0.1 r_{\text{acc}}$, and that r_{acc} is always smaller than (or at most comparable to) the Roche lobe radius.

We chose a cylindrically symmetric mass inflow condition at the outer boundary. Single particles were added to the calculation at ten points, evenly spaced around a circle of radius r_{inj} cen-

tred on the neutron star. Each particle was set moving in the azimuthal direction with specific angular momentum j , corresponding to that of a Kepler orbit of radius r_{circ} . Particles were added in this fashion at regular time intervals Δt .

We did not attempt to model the details of the disk-magnetosphere interaction, and simply used a free inner boundary at $r = r_{\text{in}}$. At the end of each time step, any particle at a radius $r < r_{\text{in}}$ was assumed to have been accreted by the central object. The mass and angular momentum of the particle was recorded, and the particle was removed from the calculation. For computational reasons, particles at very large radii $r > r_{\text{out}}$ were removed in a similar fashion. However, in this calculation the mass (and angular momentum) lost at large radii was too small (less than 1% of the total angular momentum) to significantly effect the evolution of the disk.

The temperature profile of a steady state disk was imposed upon the flow. Thus, the sound speed

$$c = c_0 \left(\frac{r}{r_{\text{circ}}} \right)^{-3/8} \quad (2)$$

where c_0 is the sound speed at the circularisation radius. We found that details of the disk's temperature profile did not significantly affect the results described below. In other words, pressure effects were not important.

In the simulation we have scaled quantities so that the mass of the accreting neutron star, M , the radius of mass addition, r_{inj} , and the Keplerian angular velocity at that radius, Ω_{inj} , are unity. The values of the various parameters used in this calculation are given in Table 1 (in terms of our scaled units).

2.3. Evolution with non-negligible viscosity

We obtained the initial condition for this calculation by running the code for $200 \Omega_{\text{inj}}^{-1}$ with mass added in an anti-clockwise direction as described above. At the end of this initialisation (time $t = 0$) the disk contained 16694 particles.

The calculation proper was started by altering the mass addition routine so that newly added material flowed in the clockwise direction (with the same magnitude j as before). The simulation was then run for a further $200 \Omega_{\text{inj}}^{-1}$.

The evolution of the disk's radial mass and angular momentum profiles from the commencement of clockwise mass addition are shown in Figs 1 and 2 respectively. The rates of mass and angular momentum accretion onto the central object are shown as functions of time in figures 3 and 4. For approximately the first $70 \Omega_{\text{inj}}^{-1}$ of the calculation, the injection streams *directly impacted* the disk, compressing it inwards. Fig 1 clearly shows the radial mass distribution becoming more strongly peaked over time, with the radius of maximum mass moving rapidly inwards. Correspondingly the mass accretion onto the central object increased to a maximum at time $t \simeq 70 \Omega_{\text{inj}}^{-1}$. This initial disk compression occurred on a timescale shorter than the outer disk's viscous timescale. The collision of the injection streams with the disk enforced a very efficient exchange of angular momentum between the two flows. The specific angular momentum of the gas at the outer edge of the disk was thus sharply reduced. This material then moved to smaller radii, with radial pressure gradients and internal viscous torques too small to prevent the disk shrinking.

Eventually, the disk was compressed to a size where the injection streams could no longer impact directly upon it. Consequently the disk shrank no further and the mass accretion dropped sharply away.

It is easy to show that a ballistic particle, launched in the azimuthal direction at radius r_{inj} with the specific angular momentum of a Kepler orbit of radius r_{circ} , will reach periastron at radius

$$r_p = \frac{r_{\text{inj}} r_{\text{circ}}}{2r_{\text{inj}} - r_{\text{circ}}}. \quad (3)$$

For our calculation, $r_p = r_{\text{inj}}/3$. Indeed, Fig 1 shows that the disk is compressed to this radius

at around $t \simeq 70 \Omega_{\text{inj}}^{-1}$. The minimum compression timescale is simply obtained by ignoring internal stresses and calculating the angular momentum that must be added to reduce the outer disk (plus newly added gas) to a circular orbit of radius r_p . For this calculation $\Delta t_{\text{min}} \simeq 30 \Omega_{\text{inj}}^{-1}$. In fact by $t = 60 \Omega_{\text{inj}}^{-1}$ all particles in the calculation remaining at radii $r > r_{\text{inj}}/3$ already had their specific angular momentum reduced below that of Kepler orbit with radius $r_{\text{inj}}/3$.

Meanwhile, the accretion streams were no longer hindered by the original disk, and were free to form a second disk. Initially a narrow ring formed at $r = r_{\text{circ}}$. Both the outer and inner ring started to spread viscously, and the inner ring began to slowly accrete through r_{in} . Once the initially almost empty gap between the two rings filled via viscous diffusion, the very strong shear between the two disks allowed angular momentum to be more efficiently extracted from the inner disk, and accelerated its demise. Hence the final drop in mass accretion was sudden rather than a gradual tailing away.

The angular momentum accretion rate in this simulation was simply proportional to the mass accretion rate as is to be expected if gas at r_{in} is still in Keplerian motion. Not until the inner disk is entirely consumed does the accretion torque on the central object change sign.

2.4. Evolution with negligible viscosity

If viscous interaction in the disk is not important, the evolution of the disk must be different from the one discussed above, in which the behaviour during the second half of the time interval modelled was dominated by viscous effects. We therefore performed further simulations with a much lower viscosity, obtained by reducing the sound speed by a factor of 5. The maximum smoothing length, $h_{\text{max}} = 0.01 r_{\text{inj}}$. As a result (see equation 1) the viscous forces are approximately a factor ten smaller than in the previous simulation.

To save computation time, we used insight gained from the previous calculation and began with two, well separated, oppositely rotating rings with identical Gaussian density profiles centred at r_{circ} and $0.5 r_{\text{circ}}$. New mass was then injected at the outer radius with a sense of rotation opposite to that of the outer ring, to simulate a second reversal of rotation at the outer boundary. Mass resolution was improved by increasing the rate of particle injection by a factor 5 over the first simulation.

In fact we completed three separate simulations for this section in order to verify that the regions of interest were being adequately resolved, and that our results were not sensitive to the numerics. The first calculation began with 16826 particles in the two rings combined. As in the previous section, particles were added at regular intervals from ten equally spaced points around a unit circle, with the points being fixed in the inertial frame. A second calculation was completed with identical system parameters but four times the mass resolution (the initial set up contained 57680 particles). The rate of **mass addition** was identical to the first simulation. A third calculation was done in which the mass resolution was identical to the first calculation but the mode of mass addition was varied. Particles were again added at ten equally spaced points around the unit circle, but each set of ten was randomly offset in azimuth. This was done to confirm that the instability described below was real and not forced by the periodic nature of the stream impact points on the outer ring. We only identified minor differences in the results of the three simulations.

The evolution of the mass distribution for the third calculation is shown in figure 5. As in the simulation described in the previous section, the outer ring moved in on the mixing timescale, but in this case it encountered the innermost ring. For this low-viscosity case, we found that the strong shear between the rings gave rise to a non-axisymmetric instability (see figure 6) that

deformed both rings severely. This instability mixed material with opposite angular momentum very effectively, so that the inner ring also fell in. The severe deformation was seen in all three simulations completed for this section. Once the outer ring reached the radius r_p and was not forced in any longer, an empty gap between the rings formed, the rings rapidly became circular again, and a new ring began forming at the circularisation radius. In figure 7 we have plotted particle neighbour number against radius for the third calculation at time $t = 3 \Omega_{\text{inj}}^{-1}$ (by which stage the rings have largely recircularised and the gap between them has formed). At this time only 260 of the 16864 particles at radii $r < 0.3 r_{\text{inj}}$ have fewer than ten neighbours. This, together with the fact that similar results were obtained in the higher resolution simulation, indicates that the calculations were not under-resolved.

We conclude from these calculations that if the externally imposed mass reversal timescale is significantly shorter than the viscous timescale at the circularisation radius, a number of concentric rings with alternating senses of rotation could be present inside the circularisation radius, down to the radius where the viscous timescale for the formation of an accretion disk or the interaction between two peaks becomes shorter than the reversal timescale.

3. Discussion

3.1. Timescales

From our results it is clear that there are two processes governing the inward transport of matter through the accretion disk. One is the usual viscosity, and the other one is mixing of material with different (or opposite) specific angular momentum. A first estimate of the relative importance of these two processes in a physical system can be found by comparing the timescales on which they can change the disk structure.

The viscous timescale for a standard disk is

given by

$$\tau_v \sim \frac{r^2}{\alpha c_s h} \sim 7 \times 10^6 \alpha_{0.1}^{-1} r_{10}^{\frac{3}{2}} \left(\frac{h}{r}\right)_{0.01}^{-2} \text{ sec}, \quad (4)$$

in which $\alpha_{0.1}$ is the Shakura-Sunyaev viscosity parameter in units of 0.1, r_{10} the radius in units of 10^{10} cm, and h is the thickness of the disk. For a system like GX 1+4 this timescale is of the order of 7000 years if we assume that the disk forms at a radius of about $0.1 r_{\text{acc}} \sim 10^{13}$ cm. Note that counter-rotating rings will interact viscously on a timescale shorter than that given by the expression above, and can be estimated by replacing h/r by h/l , where l is the separation between the two peaks

The typical timescale on which the inflow conditions at the outer boundary conditions can change due to the flip-flop instability is

$$t_{ff} \sim \frac{GM}{v_w^2 c_{s,w}} \sim 9 \times 10^7 v_{w,15}^{-2} c_{s,10}^{-1} \text{ sec} \quad (5)$$

in which $v_{w,15}$ is the wind speeds in units of 15 km/s, and $c_{s,10}$ the sound speed in the wind in units of 10 km/s. The timescale needed by the dynamical processes associated with the change in boundary conditions to cause the disk structure to change significantly must be the same as t_{ff} , since a significant change requires mixing material already present in the disk from the previous episode with a similar amount of material with different angular momentum.

Again for the parameters of GX 1+4, we expect a steady viscous disk to form when $t_v < t_{ff}$, implying $r < 5 \times 10^{10}$ cm if α and h/r have their typical values. For the pulsars accreting from a fast wind this limit corresponds to $r < 10^8$ cm, which is smaller than or comparable to the magnetospheric radius so that in these cases viscous forces must play a negligible role in the accretion flow even if a disk forms.

These considerations led us to examine two cases in the numerical simulations. In the first, the viscosity was so large that it governed the

evolution near the inner boundary of the computational domain, which modelled the transition from the mixing dominated to the viscosity dominated regime at small radii. The second simulation addressed what happens in the outer parts of the disk where viscosity is unimportant. In both cases we found that it is always the externally imposed timescale that determined the timescale of changes at the inner boundary. If the viscosity was low, leading to a viscous timescale much longer than the external reversal time, dynamical effects took over to transport the material inward. This appears consistent with the long-term observed behaviour of GX 1+4.

3.2. Mass and angular momentum accretion rates

The mass and angular momentum rates shown in figures 3 and 4 vary relatively smoothly. This is to be expected as long as the disk is so large that its inner part is a steady viscous disk, which will smear out any more abrupt changes over a viscous timescale, which in turn is comparable to the externally imposed timescale as discussed above. These profiles should be fairly universal as long as viscosity is important close to the magnetosphere, since the non-viscous evolution simply pushes in a sequence of rings, with the inner one disappearing by forming a disk and being accreted as in our first simulation.

The simulations indicate that a reversal of the material accretion torque should occur during a period of *low* luminosity. There may be some evidence for this in the data for GX 1+4, especially the non-detection of the source when its long-time spin rate change reversed in 1984, or possibly the low luminosities just before and after the 1994-1995 spin-up episode observed by BATSE (Chakrabarty et al. 1997). Although the timescales of these two observed features differ by a factor of 10, it is not inappropriate to apply the same model to them, since the timescale quoted in equation 5 for the change of the outer boundary condition is only typical, and shorter

and longer timescales have been seen in calculations of the flip-flop model. An alternative explanation put forward by Cui (1997) invokes a “magnetic propeller” mechanism to explain the low accretion episode of GX 1+4.

We do not intend that this model explain all details of the observations of torque and luminosity in GX 1+4, which sometimes show the same torque for very different luminosities even when the disk is supposedly rotating in the same direction as evidenced by the short-term torque-luminosity correlation. Clearly an additional model for the interaction between disk and magnetosphere and the associated braking torques is required.

4. Concluding Remarks

We are of course fully aware of the extreme simplifications that were used in our simulations. In more realistic studies, 3-dimensional effects such as subsequent bursts of material arriving at the outer boundary not being coplanar or not having exactly opposite angular momentum, or vertical motion due to the strong heating that must occur in the strong shearing regions should be included. We plan to address some of these in future work.

We expect, however, that two main effects will remain standing even after more detail has been included. The first is that changes at the magnetospheric radius occur on a similar timescale as changes at the outer boundary, and the second is that rings with opposite rotation do not tend to mix completely but rather create a gap between themselves, leading to the prediction that torque reversals should occur during minima in accretion luminosity.

The authors would like to thank Dayal Wickramasinghe and Phil Armitage for comments and discussions.

REFERENCES

Baykal, A. & Ögelman, H. 1993, A&A 267, 119

Bildsten, L., et al., 1997, ApJS, 113, 367

Chakrabarty, D. & Roche, P. 1997, ApJ, 489, 254

Chakrabarty, D., et al., 1997, ApJ, 481, L101

Cui, W., 1997, ApJ, 482, L163

de Kool, M. & Anzer, U. 1993, MNRAS, 262, 726

Dotani, T., Kii, T., Nagase, F., Makishima, K., Ohashi, T., Sahao, T., Koyama, K., Touhy, I.R., 1989, PASJ, 41, 427

Fryxell, B.E. & Taam, R.E., 1988, ApJ, 335, 862

Fryxell, B.E. & Taam, R.E., 1989, ApJ, 339, 297

Ghosh, P., Lamb, F.K., 1979, ApJ, 234, 296

Greenhill, J.G., et al., 1989, A&A, 208, L1

Li, J. & Wickramasinghe, D.T., 1998, MNRAS, in press

Lovelace, R.V.E., Chou, T., 1996, ApJ, 468, L25

Makishima, K., et al., 1988, Nature, 333, 746

Matsuda, T., Inoue, M., Sawada, K., 1987, MNRAS, 226, 785

Monaghan, J.J., 1992, ARA&A, 30, 543

Murray, J.R., 1996, MNRAS, 279, 402

Murray, J.R., 1998, MNRAS, 297, 323

Murray, J.R., Armitage, P.J., 1998, MNRAS, 300, 561

Nagase, F. 1989, PASJ, 41, 1

Nelson, R.W., et al., 1997, ApJ, 488, L117

Ruffert, M., 1992, A&A, 265, 82

Ruffert, M., 1997, A&A, 317, 793

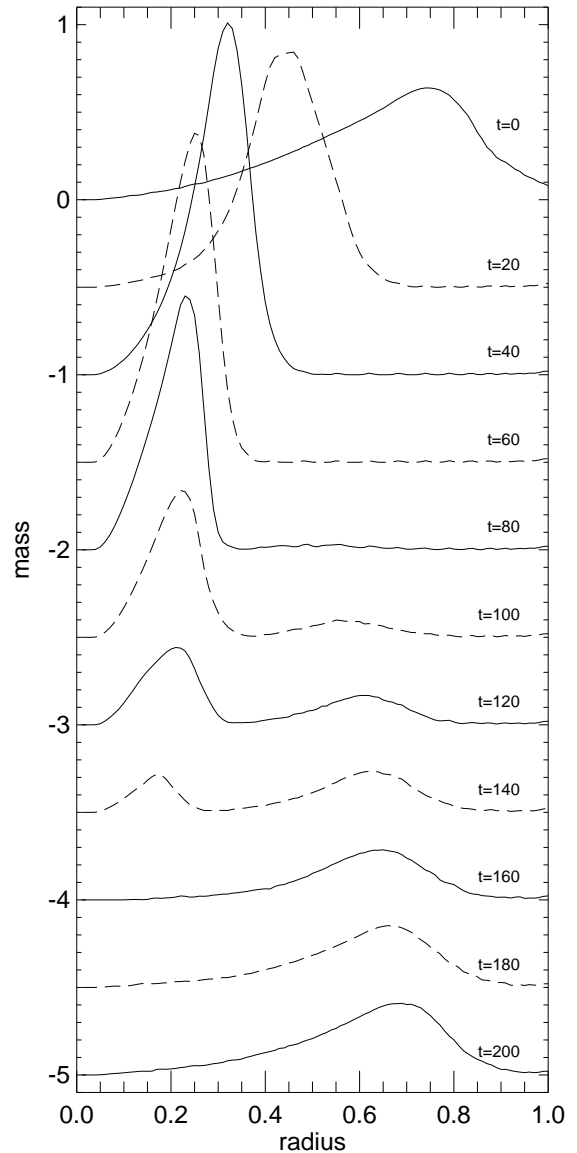


Fig. 1.— Mass as a function of radius for the high viscosity calculation (section 2.2), at the times shown. The angular velocity of mass added at the outer boundary is reversed at $t = 0$ (topmost curve). Subsequent curves are offset 0.5 units in mass. Every second curve is dashed for clarity.

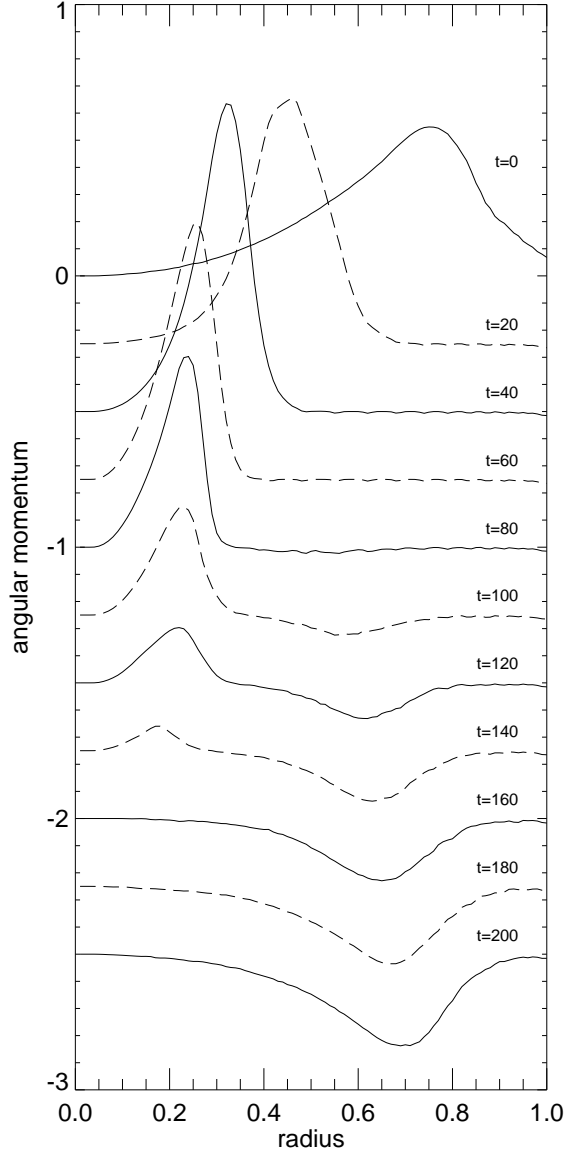


Fig. 2.— Angular momentum as a function of radius for the high viscosity calculation. Every second curve is dashed for clarity.

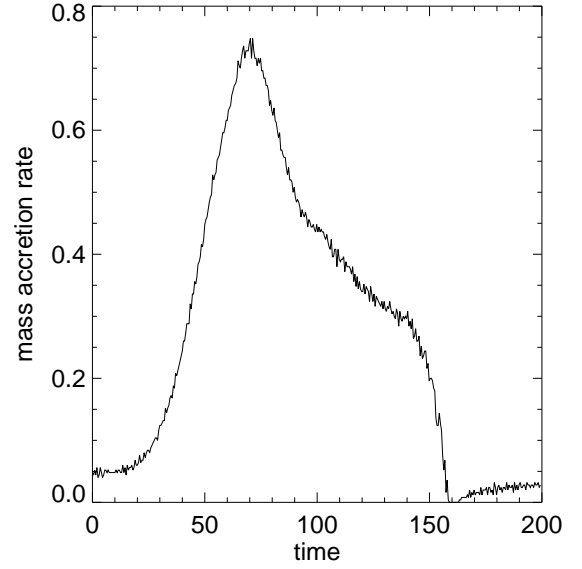


Fig. 3.— Mass accretion rate as a function of time for the high viscosity calculation.

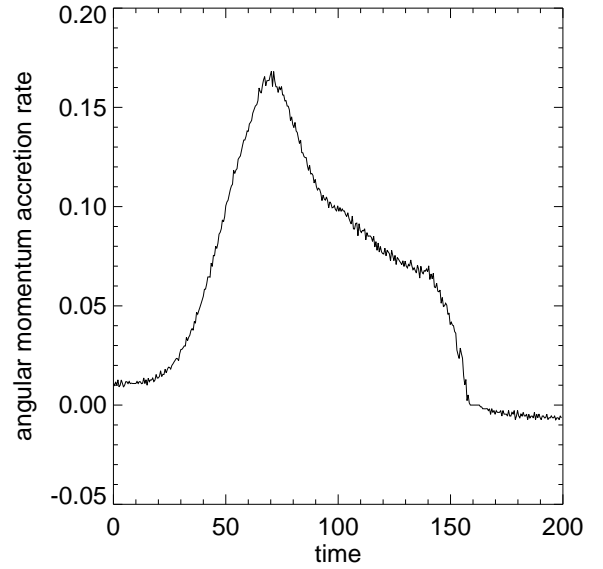


Fig. 4.— Angular momentum accretion rate as a function of time for the high viscosity calculation.

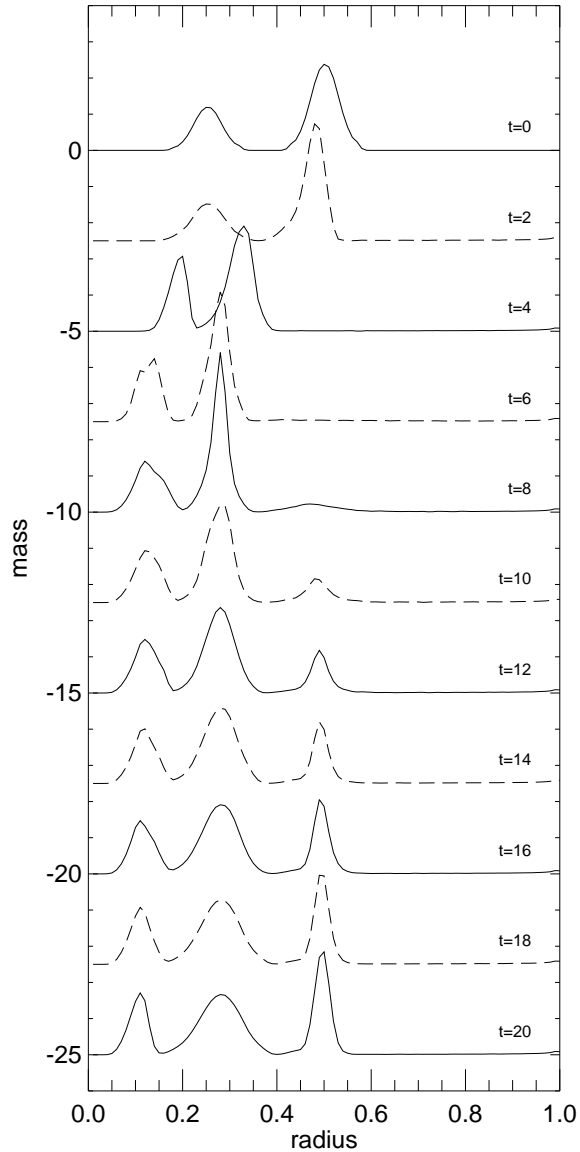


Fig. 5.— Evolution of the radial mass profile for the third calculation with negligible viscosity (section 2.3) in which mass injection was “disordered” (i.e. the azimuth of each set of ten particles was set randomly). The calculation begins ($t = 0$) with two counter-rotating Keplerian annuli with identical Gaussian density profiles centred at $r = 0.25$ and $r = 0.5 r_{\text{out}}$.

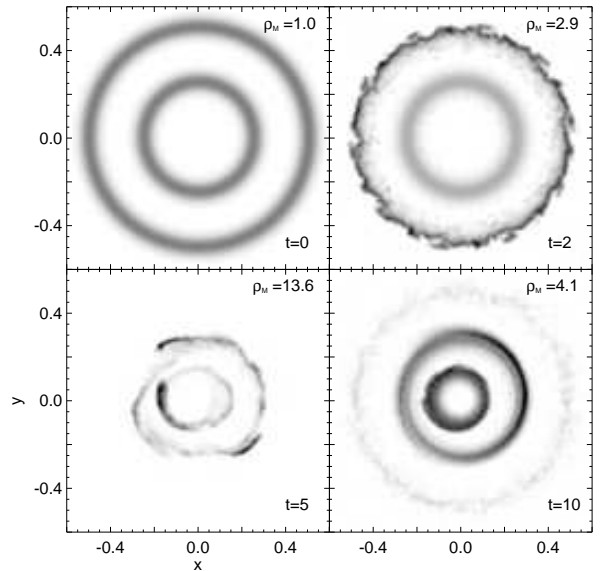


Fig. 6.— Density maps of the “disordered injection” negligible viscosity calculation shown in figure 5. In order to show as much detail in each frame, the maps have been separately scaled. The maximum density and time of each snapshot are shown in the top and bottom right respectively of each panel.

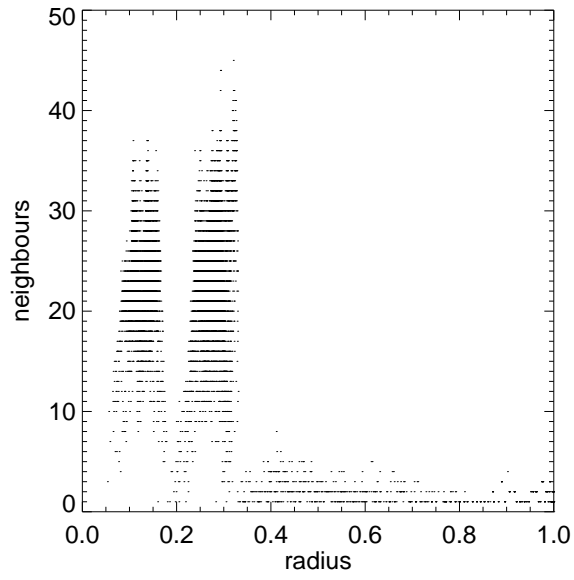


Fig. 7.— Neighbour number plotted against radius for each particle at $t = 3 \Omega_{\text{inj}}^{-1}$ in the negligible viscosity simulation with “disordered” mass injection.

TABLE 1
PARAMETER VALUES

Parameter	c_0	h_{\max}	r_{in}	r_{circ}	r_{out}	Δt
Units	$r_{\text{inj}} \Omega_{\text{inj}}$	r_{inj}	r_{inj}	r_{inj}	r_{inj}	Ω_{inj}^{-1}
Value	0.1	0.02	0.05	0.5	1.2	0.10
